Water temperature and concentration measurements within the expanding blast wave of a high explosive

2011 Meas. Sci. Technol. 22 045601

(http://iopscience.iop.org/0957-0233/22/4/045601)

Report Documentation Page

Form Approved
OMB No. 0704-0188

1. REPORT DATE	2. REPORT TYPE	3. DATES COVERED
FEB 2011		**00-00-2011 to 00-00-2011**

4. TITLE AND SUBTITLE	5a. CONTRACT NUMBER
Water temperature and concentration measurements within the expanding blast wave of a high explosive	5b. GRANT NUMBER
	5c. PROGRAM ELEMENT NUMBER
6. AUTHOR(S)	5d. PROJECT NUMBER
	5e. TASK NUMBER
	5f. WORK UNIT NUMBER
7. PERFORMING ORGANIZATION NAME(S) AND ADDRESS(ES) **Naval Surface Warfare Center,Indian Head Division,Research and Technology Division,Indian Head,MD,20640**	8. PERFORMING ORGANIZATION REPORT NUMBER
9. SPONSORING/MONITORING AGENCY NAME(S) AND ADDRESS(ES)	10. SPONSOR/MONITOR'S ACRONYM(S)
	11. SPONSOR/MONITOR'S REPORT NUMBER(S)

12. DISTRIBUTION/AVAILABILITY STATEMENT
Approved for public release; distribution unlimited

13. SUPPLEMENTARY NOTES

14. ABSTRACT

We present an application of absorption spectroscopy to directly measure temperature and concentration histories of water vapor within the expansion of a high explosive detonation. While the approach of absorption spectroscopy is well established, the combination of a fast near-infrared array, broadband light source, and rigid gauge allow the first application of time-resolved absorption measurements in an explosive environment. The instrument is demonstrated using pentaerythritol tetranitrate with a sampling rate of 20 kHz for 20 ms following detonation. Absorption by water vapor is measured between 1335 and 1380 nm. Water temperatures are determined by fitting experimental transmission spectra to a simulated database. Water mole fractions are deduced following the temperature assignment. The sources of uncertainty and their impact on the results are discussed. These measurements will aid the development of chemical-specific reaction models and the predictive capability in technical fields including combustion and detonation science.

15. SUBJECT TERMS

16. SECURITY CLASSIFICATION OF:			17. LIMITATION OF ABSTRACT	18. NUMBER OF PAGES	19a. NAME OF RESPONSIBLE PERSON
a. REPORT **unclassified**	b. ABSTRACT **unclassified**	c. THIS PAGE **unclassified**	**Same as Report (SAR)**	**11**	

Meas. Sci. Technol. **22** (2011) 045601 (10pp) doi:10.1088/0957-0233/22/4/045601

Water temperature and concentration measurements within the expanding blast wave of a high explosive

J R Carney[1], J M Lightstone[1], S Piecuch[2] and J D Koch[2]

[1] Indian Head Division, Naval Surface Warfare Center, Research and Technology Division, Indian Head, Maryland, USA
[2] Mechanical Engineering Department, Marquette University, Milwaukee, WI, USA

E-mail: jon.koch@marquette.edu

Received 2 November 2010, in final form 8 February 2011
Published 15 March 2011
Online at stacks.iop.org/MST/22/045601

Abstract
We present an application of absorption spectroscopy to directly measure temperature and concentration histories of water vapor within the expansion of a high explosive detonation. While the approach of absorption spectroscopy is well established, the combination of a fast, near-infrared array, broadband light source, and rigid gauge allow the first application of time-resolved absorption measurements in an explosive environment. The instrument is demonstrated using pentaerythritol tetranitrate with a sampling rate of 20 kHz for 20 ms following detonation. Absorption by water vapor is measured between 1335 and 1380 nm. Water temperatures are determined by fitting experimental transmission spectra to a simulated database. Water mole fractions are deduced following the temperature assignment. The sources of uncertainty and their impact on the results are discussed. These measurements will aid the development of chemical-specific reaction models and the predictive capability in technical fields including combustion and detonation science.

Keywords: absorption spectroscopy, water, detonation, combustion

(Some figures in this article are in colour only in the electronic version)

1. Introduction

1.1. Background

Experimental detonation science research has historically relied on a limited number of *in situ* measurements for evaluating rates, efficiencies, and effects of the processes. High-speed photography, pressure measurements, and velocity measurements have long been staples of the field [1, 2]. The application of species-specific optical techniques to detonation experiments has evolved more recently. Streak cameras have been used to observe the optical emission signatures of detonation and post-detonation combustion events to learn about relative trends in the energy release rates [3–5]. Emission-based temperature measurements, typically in the form of pyrometry, can also offer sufficient time resolution for detonation studies, but like other emission techniques, they can be difficult to interpret in terms of spatial location and quantitative accuracy [3, 6]. As a result, these measurements are difficult to directly compare with simulations. Improving the temporal and spatial resolution of species-specific measurements would give more direct access to thermal properties within these harsh environments and would provide a new level of detail by which to compare and refine computational codes.

Absorption techniques can provide species-specific, high-rate data from a well-defined volume and have been successfully applied in environments such as pulse detonation engines [7, 8], internal combustion engines [9, 10], and shock tubes [11–13]; however, their application to the free field expansion of the blast following the detonation of energetic materials has been sparse, perhaps due to the difficulties involved in signal acquisition in the midst of the post-detonation environment. In one exception, Carney *et al*

measured atomic aluminum absorption lines in the visible region (390–400 nm) using light from an exploding argon discharge as a source and a spectrometer coupled to a streak camera for detection [14]. While this represents the first known achievement of absorption measurements in this experimental arrangement, the data were ultimately limited by the 100 μs duration of the light source and the necessity of an assumed temperature of the flow. Glumac [15] recently demonstrated the use of a Nd:YAG pumped dye laser for absorption measurements (single shot per detonation experiment, 10 ns temporal resolution) following ignition of exploding bridge wires and milligram charges of nanothermite composites. Temperature measurements from titanium bridgewires did not indicate thermal equilibrium among the probed electronic states of Ti atoms, but the time at which this measurement occurred after detonation was not mentioned.

This paper presents simultaneous measurements of water vapor temperature and concentration histories using absorption spectroscopy in the supersonic expansion regime following the detonation of a high explosive. Water vapor was used as an absorber molecule because it is a major product of many detonation and combustion reactions and thus does not require additional doping of the formulation which may alter the energy release process. Water also has absorption features in a region where telecommunication devices often operate, making light sources and fiber components readily available. A rigid mechanical gauge was designed to protect the optical components and hold them fixed in order to obtain transmission data even during the passage of the shock wave. Transmission measurements were acquired at a rate of 20 kHz for 20 ms. Molecular temperatures and concentrations were determined by fitting the measured transmission spectra to simulated water spectra, resulting in a measurement that begins before the leading shock passes the measurement volume and extends until the atmosphere has nearly returned to standard conditions. These measurements and the continued development of such approaches will be useful for refining our understanding and our ability to simulate detonation and high-rate combustion events.

1.2. Absorption spectroscopy theory

The theory of absorption spectroscopy has been detailed previously [11, 16]. The Beer–Lambert law (equation (1)) can be used to describe the transmission of light through an optically thin, uniformly absorbing medium. This law states that the spectral transmission ratio T_ν is a function of the spectral absorption coefficient k_ν (cm^{-1}) and the path length L (cm), where I and I_o are the transmitted intensity and initial intensity at a specific frequency, ν. The product $k_\nu L$ is also known as absorbance (α_ν) and can be expressed as a function of several key properties as shown in equation (2):

$$T_\nu = \left(\frac{I}{I_o}\right)_\nu = \exp(-k_\nu L), \tag{1}$$

$$\alpha_\nu = k_\nu L = P\chi_i S_i(T)\varphi_\nu L. \tag{2}$$

In equation (2), P is the total pressure (atm), χ_i is the mole fraction of the absorbing species, ϕ_ν (cm^{-1}) is a normalized lineshape function and $S_i(T)$ (cm^{-2} atm^{-1}) is the linestrength of the isolated transition at the temperature T (K). The lineshape function, ϕ_ν, reflects the variations in relative strength of a single transition with respect to frequency and is generally influenced by temperature, pressure, and gas composition. Many physical mechanisms influence the lineshape function; however, only two dominant broadening mechanisms are considered for the research in this work: Doppler (velocity) and collisional (pressure) broadening. Transmission spectra are, therefore, sensitive to thermodynamic properties (temperature (T), mole fraction absorber (χ_i), and pressure (P)) in the probed path length, which can be exploited to obtain fast, *in situ* property measurements that are species specific.

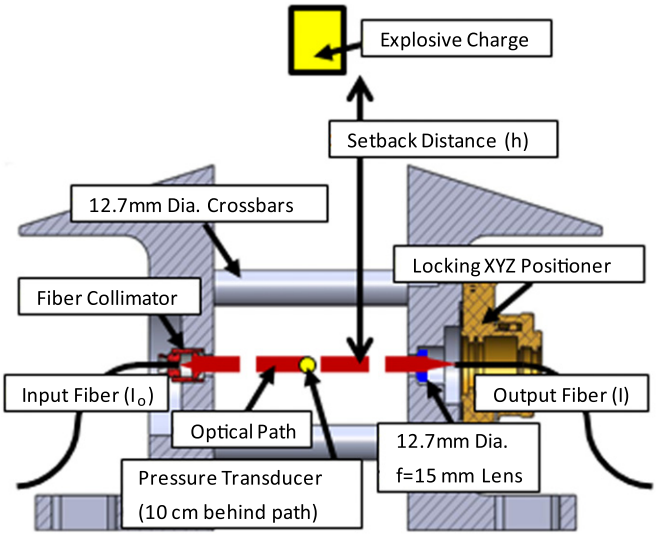

Figure 1. Cross-sectional view of the absorption gauge used to measure light absorption within the blast wave of a detonation. Single-mode fibers attached to the fiber collimator (left, input or pitch fiber, I_o) and a three-axis locking lens positioner (right, output or catch fiber, I).

2. Experiment

2.1. Absorption spectroscopy gauge for detonation experiments

One of the challenges to implementing quantitative absorption in close proximity to the detonation environment is the mechanical alignment and protection of the necessary optics. The gauge, whose cross-section is shown in figure 1, was designed for such experiments. The housing was made of 1018 steel, and the gauge roof was extended to shield the opto-mechanical components from the primary blast wave. The input fiber (pitch fiber, I_o) was coupled via a fiber collimator with a focal length of 8 mm and numerical aperture of 0.55 (Thorlabs F240FC-C). A short focal length here minimized atmospheric water absorption in the protected space between the fiber and lens. Transmitted light was coupled to the single-mode output fiber (catch fiber, I) using a 12.5 mm diameter 15.0 mm focal length lens (Thorlabs LA1540-C), which was held by a locking three-axis positioner (Newport

LP-05A-XYZ). This three-axis lens positioner allowed for alignment of the catch fiber and had a sufficiently strong locking mechanism to minimize the potential for movement of the fiber with respect to the lens. It was determined that a single mode fiber must be used on the catch side in these experiments because the noise induced by a multi-mode fiber was greater than the measurable absorption signal. The resolution of the spectrometer would also be compromised by the use of a larger catch fiber.

From the light source, roughly 20 mW of near-infrared (NIR) light was passed from the single-mode fiber to the pitch end of the gauge. Adjusting the alignment of the catch fiber to the optimal coupling position, a maximum coupling efficiency of ∼10% (2 mW) was achievable. In an attempt to minimize the loss of transmission due to beam steering and absorption gauge vibrations, the catch fiber was positioned slightly further from the lens than the optimal coupling position allowing a coupling efficiency of ∼3% (0.6 mW). Although this reduced the amount of light entering the fiber, coupling of the light was sustainable even with slight transverse translation of the beam with respect to the focusing lens, up to about 85 μm, as measured by a micron stage. The path length for these experiments, 15 cm, was defined by the length between the two lenses. This design incorporated 12.7 mm diameter crossbars and slight interference fits to ensure the rigidity of the structure and minimize the relative motion of the pitch and catch optics. The four crossbars were positioned off-center with respect to the gauge body, allowing the passage of a blast wave and combustion products with minimal interference from reflective surfaces. The crossbars were also removable so the path length could be varied. A variable path length was particularly sought because the degree of beam steering and attenuation due to non-molecular absorption or scattering was largely unknown prior to these experiments. Furthermore, other light sources and detectors can be used with this gauge to probe other molecules with different transition strengths, and they would require different path lengths for maintaining adequate signal-to-noise.

2.2. Explosive configuration

Explosive experiments were conducted at the Sigmund J Jacobs Detonation Science Facility at the Indian Head Division, Naval Surface Warfare Center. A bombproof chamber approximately 30 kL in volume was used to contain the detonation experiments. As shown schematically in figure 2, the sensitive instrumentation and other experimental equipment were kept in an adjacent room, shielded from the bombproof chamber, and electrical and optical signals were transmitted via wires and fibers, respectively. The explosive charge assembly was suspended directly above the absorption gauge and centered with respect to the optical path. The bottom surface of the charge was set at a specified height of 8, 15, or 23 cm above the center of the optically probed volume with an approximate error in height of ±1 mm, as indicated by the '*h*' dimension in figure 1. This separation between the charge and the optical path is referred to as the 'setback distance' in the discussion below. The charge assembly consisted of an

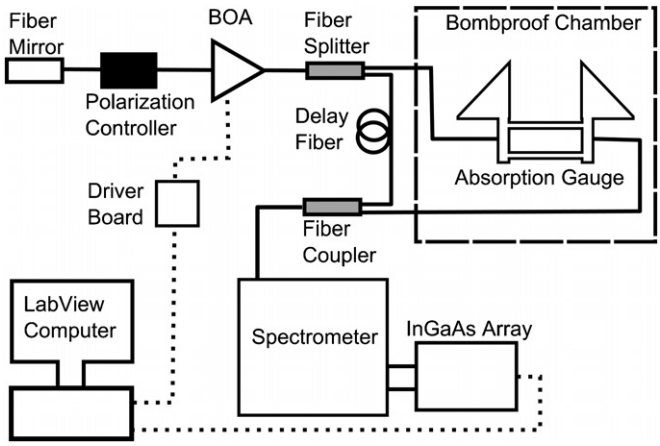

Figure 2. Schematic of the optical layout of the absorption spectroscopy experiment. NIR light was generated by a BOA and coupled to a fiber mirror on one end and a fiber coupled beam splitter on the other. The splitter sent 90% of the light to the blast chamber where it was pitched and focused onto another fiber which carried it out of the chamber. The other 10% was transmitted through a delay line and both signals were sent to the spectrometer via a second coupler. The spectrometer/array combination was controlled by the DAQ system to acquire one transmission spectrum (I/I_{ref}) every 50 μs (20 kHz repetition rate).

RP-3 exploding bridgewire detonator (Teledyne RISI, 29 mg pentaerythritol tetranitrate (PETN)) and the main charge, which was either 12.7 or 25.4 mm right circular cylinders of PETN. The PETN charges were pressed to near theoretical maximum density, weighing 2.6 or 21 g for the 12.7 and 25.4 mm cylinders, respectively. A thin layer of vacuum grease was applied to the face of the detonator so that the main charge would stick to the surface without the need for other adhesives. Care was taken to construct the explosive assembly out of pure PETN so as to limit the amount of contaminants and optimize the light transmission through the expanding cloud since PETN has been shown to detonate to optically clear gas products. To fire the charges, a 500 V pulse generator was used to initiate the detonator with a controlled TTL pulse from a digital delay generator (Stanford Research Systems, DG535). The delay generator also sent a timing pulse to a computer with a LabView-based data acquisition (DAQ) system, which controlled the timing of the optical pulses and data collection (described below).

2.3. Optical and DAQ configuration

The system reported here was assembled to minimize polychromatic beating noise in fast spectrometer measurements through use of a split-pulse referencing scheme, following previous work [17]. Figure 2 presents a schematic of the optical layout of the experiment. A booster optical amplifier (Covega BOA 1036) was the NIR source, capable of generating light in the 1310–1390 nm region, which contains lines from the ν_1+ν_3, the $2\nu_1$, and the $2\nu_3$ bands of H_2O. One end of the BOA was coupled to a fiber mirror to amplify the optical output. Some of the components including the BOA, fiber couplers, and diffraction grating were polarization sensitive, so a polarization controller was

placed in between the BOA and the fiber mirror to provide some control over these effects and maximize the signal quality in the wavelength region of interest. The BOA was activated by a diode laser driver board (Micro Laser Systems DBDL2000T/S) and cooled by a thermo-electric cooler (Inphenix IPEVM1010). The driver board was triggered by LabView via a field-programmable gate array card (National Instruments PCI-6601). The light from the BOA was sent to a beam splitter which sent 10% of the signal through an ≈5 km delay line and 90% of the signal to the blast chamber. The delay line temporally separated the two signals and allowed a single detector to record both signals. As noted by Sanders *et al*, this split-pulse scheme minimized polychromatic beating noise and removed challenges associated with comparing signals from two different detectors such as bias and differing spectral responses [17]. Although there were still some differences between the reference and transmitted signals due to polarization changes and the separate fibers and lenses used, they were small enough to have little effect on the data reduction scheme. 90% of the light from the BOA was sent to the blast chamber via a 10 μm diameter, 15 m long, single-mode fiber (Corning SMF-28e). In the blast chamber, the light was pitched across the absorption gauge where the water vapor measurement was made.

The transmitted light was directed out of the blast chamber with a single-mode fiber (Corning SMF-28e) and re-coupled with the delay line before entering the spectrometer. The slit on the spectrometer was opened to 600 μm, allowing all light from the 10 μm diameter fiber to enter the spectrometer (Andor Shamrock 303-i). A 1000 g mm^{-1} grating blazed at 1.3 μm was used in the spectrometer. The spectral resolution was 0.093 nm or ≈2 pixels, FWHM, and a range of ∼45 nm was achieved across the InGaAs array. This spectrometer–array combination is also described in recent work where it was used to record emission signals from a detonation event [18]. The spectrometer was continually purged with nitrogen gas during these experiments to eliminate excess water absorption along the light path within the spectrometer.

The detector array (Goodrich Sensors Unlimited Inc., SU-LDH Digital Line Scan Camera) was controlled by the same LabView program that controlled the BOA. For each light pulse from the BOA, two spectra were recorded: the transmitted signal I and the reference delay fiber signal I_{ref}. The BOA was fired at a rate of 20 kHz while the camera collected the transmitted and delayed signals at a rate of 40 kHz. The light pulse duration and timing were optimized to match the duty cycle of the camera and prevent multiple signals (i.e. both I and I_{ref}) from being recorded in a single frame. Resultant transmission spectral pairs (I and I_{ref}) were recorded every 50 μs. The entire acquisition process was triggered by the charge firing circuitry, which sent signals to the LabView program.

As described below, the methods of Kranendonk *et al* [16] were used to deduce the temperature and mole fraction from the data acquired with this instrument. While this method could potentially be used for simultaneous pressure measurements, the resolution of the spectrometer was insufficient for the determination of pressure since it depends primarily on the lineshape function in flows of unknown mole fraction. The pressure was thus measured simultaneously with the optical measurement via a Kulite pressure transducer (XTEL-190-500A) located 10 cm behind the optical path and aligned with the center of the optical path as indicated in figure 1. The pressure data were used as an input to the post-processing procedure to deduce the temperature.

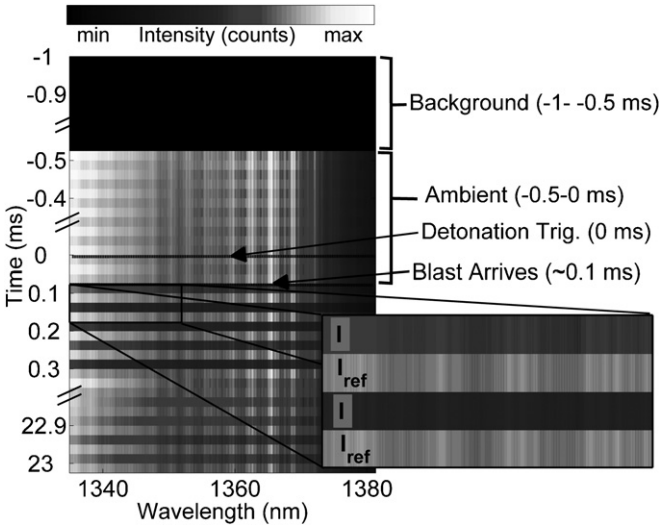

Figure 3. Image of raw data collected during one experiment from the detonation of a 2.6 g PETN pellet placed 23 cm from the absorption gauge. Time progresses from top to bottom with the trigger to detonation as the reference time ($t = 0$ ms), and wavelength is listed on the horizontal axis. A legend of the relative intensity color contours used is presented at the top of the figure. The collection began with background spectra with the source off, followed by ambient measurements with light source on near $t = -0.5$ ms. The detonation was triggered near $t = 0$ ms and the shock arrived at the path length of the gauge at $t = 0.1$ ms. The decrease in transmitted intensity can be used to resolve the transmission (I) and reference (I_{ref}) collections.

2.4. Data collection, reduction, and analysis

A raw image produced from the spectrometer is presented in figure 3. (All data in figures 3–7 are from the same detonation experiment.) This image was captured during the detonation of a 2.6 g PETN pellet at a setback distance of 23 cm. The detonation trigger was used as the reference time ($t = 0$ ms) in these figures. The camera was triggered 1 ms prior to detonation to capture background signals, represented by the dark area at the top of figure 3. After about 0.5 ms (0.5 ms prior to detonation), the light source was triggered, supplying pulses of light ≈20 μs in duration at a rate of 20 kHz to the optical fibers. The light from the gauge hit the camera first (I) followed by the light from the reference line (I_{ref}) 25 μs later. A set of spectra that measured ambient humidity conditions was then recorded. The charge was detonated at $t = 0$ ms as shown by a dashed line in figure 3. Following this detonation, a sharp decrease in transmission intensity was observed (∼0.1 ms after detonation trigger), attributed to the arrival of the shock front at the absorption path. The transmission intensity at this time fell to around 50% for one or two measurements due to a combination of absorptive and beam steering losses. Typically,

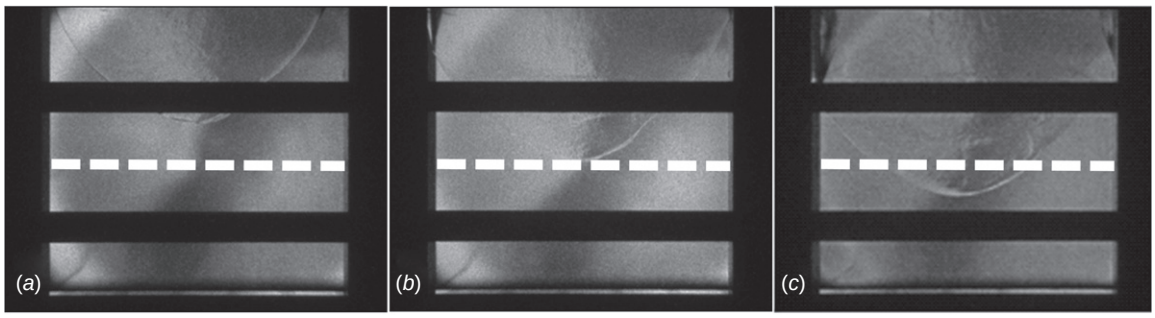

Figure 4. A set of three consecutive digital shadowgraphs of a shock front expanding through the absorption gauge, corresponding to the $t = 0.1$ ms delay in figure 3. The spatial position of the path length (15 cm long) is marked by the dashed, white line in each image. The shock front is originating from the charge at a setback distance of 23 cm and is traveling from top to bottom. The interframe and exposure times of the images were 10 μs and 20 ns, respectively.

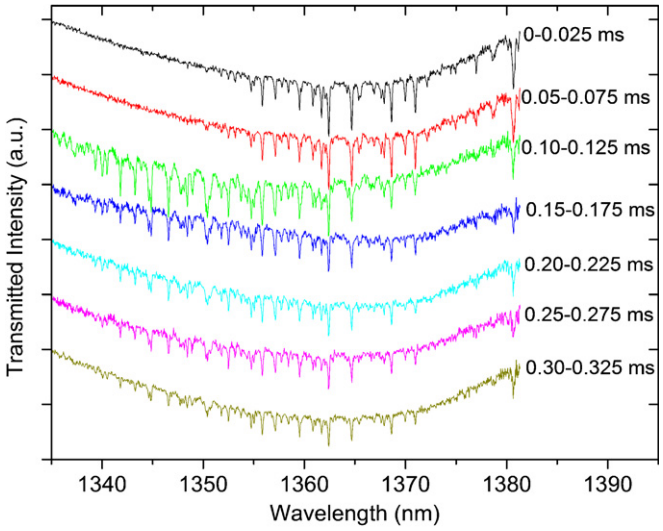

Figure 5. Transmission spectra (I/I_{ref}) from the data in figure 3, recorded during an experiment with a 2.6 g charge of PETN, suspended at a setback distance of 23 cm. Spectra are offset vertically such that time is advancing from top to bottom and the time-stamp describing each measurement (I) is displayed to the right of each spectrum.

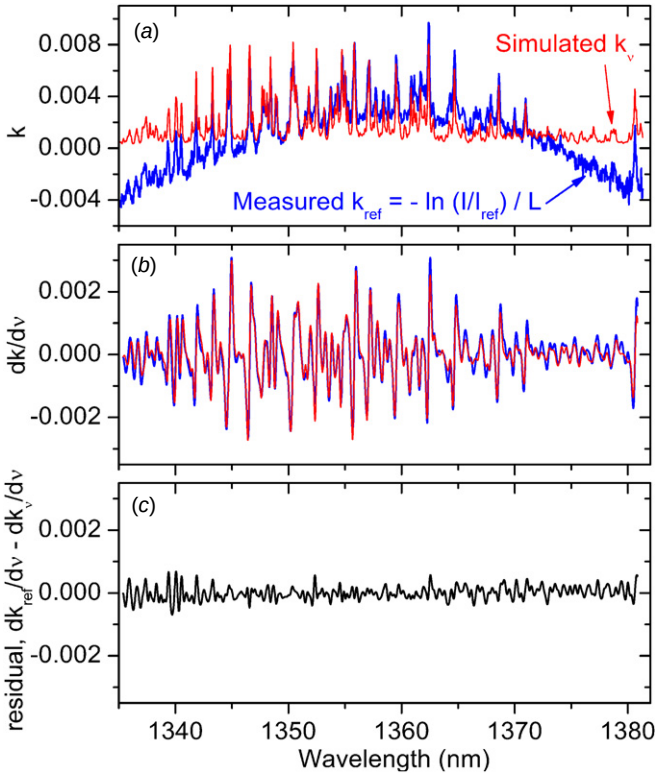

Figure 6. A sample measured spectrum captured 0.1 ms after the detonation of a 2.6 g PETN pellet placed 23 cm from the absorption gauge is used to exhibit the steps to prepare simulated and measured spectra for comparison. (*a*) Measured and simulated absorption spectra based on I/I_{ref} where the measured spectrum exhibits a slowly drifting increase and decrease in the baseline, attributed to polarization effects in the optical system, (*b*) measured and simulated spectra after smoothing subsequent differentiation, and (*c*) residual difference between measurement and simulation of a smoothed, differentiated spectrum. The temperature of the simulated spectrum is 1300 K.

transmission values of 80% or higher were observed for the remainder of the collection time.

Figure 4 presents a set of three digital shadowgraphs that were recorded simultaneously with the data presented in figure 3. The refractive index change associated with the shock front from the expanding blast results in a refraction of the collimated backlight and, therefore, helps to resolve the position of the shock front (moving from top to bottom on the images). These images were recorded with an interframe time of 10 μs and an exposure time of 20 ns. The position of the optical path is marked using the dashed white line on each image. The shock begins to pass into the absorption region in figure 4(*b*). The dark regions of each image indicate the steel frame and support crossbars of the gauge. This set of images provides a sense of the speed with which the shock was traveling through the gauge during the experiment. Based on the interframe time and the distance covered, the bottom of the shock wave was traveling approximately 2 mm μs^{-1} when these images were acquired.

In figure 5, transmission spectra were calculated from the ratio of transmitted intensity (I) and reference intensity (I_{ref}) from the image in figure 3. The spectra are offset vertically in figure 5 for clarity, presenting increasing time from top to bottom. Each spectrum represents a 25 μs integration time with 25 μs in between each spectrum (for

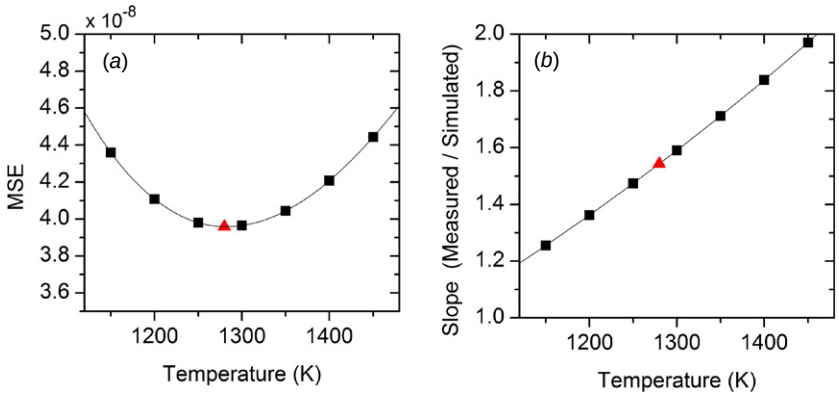

Figure 7. (*a*) MSE versus simulated temperatures from the data presented in figure 6. The squares were calculated from the sum-squared residual difference between measured and calculated spectra in the database. The line is the quadratic fit through the squares, and the triangle is the prediction of the temperature for the measured spectrum with the minimum MSE. (*b*) Slopes of the best-fit lines of the measured versus simulated data curve fit at the corresponding simulated temperatures. Squares are calculated from spectra in the database. The triangle is the predicted slope for the best-fit line of the measured spectrum. The value of the slope at the best-fit temperature is the scaling factor used to calculate the mole fraction of water vapor.

measurement of the reference intensity). While the overall transmission was between 50% and 100% relative to the pre-shock conditions, the maximum molecular absorption (the size of the water vapor peaks) was around 4–6% more than the baseline. The first (top) spectrum in figure 5 shows absorption due to the room temperature water present in the air before the shock front arrives. Absorption lines on the blue side of the spectrum appear with the passage of the shock front, showing an increase in the population of higher rotational states and corresponding to a higher temperature. Water temperatures and mole fractions of the expanding PETN blast wave were extracted from sets of transmission spectra such as those shown in figure 5.

The data reduction procedure to determine temperatures and mole fractions of water vapor from the spectra followed the method described in detail by Kranendonk *et al* [16]. It consisted of finding the simulated water spectrum that best matched the measured spectrum. First, a database of simulated H_2O absorption spectra was generated at relevant conditions using the locations and linestrengths from Barber *et al* [19]. From the line list, a database of spectra was created for $T =$ 250–3500 K in increments of 50 K and $P =$ 0.8–6.5 atm in increments of 0.1 atm, all for a fixed mole fraction of 0.21. This mole fraction was chosen as a starting point as the equilibrium detonation products of PETN are predicted to be 0.21 mole fraction water. The lineshapes in the spectra were modeled using a numerical approximation for a Voigt profile that incorporates Doppler and collisional broadening [20]. Collisional broadening coefficients were taken from Kranendonk *et al* [16] and collision widths were calculated based on the pressures measured during the experiment. The measured spectra were wavelength-calibrated by iteratively comparing a measured spectrum with a simulated spectrum at the same conditions. The calibration was first performed using the pre-shock wave (room temperature) data for each experiment. Strong absorption peaks were chosen as reference points on both the measured and simulated spectra. A quadratic polynomial was fit through the measured versus simulated reference points and used to calibrate the wavelength axis. It was found, however, that there are notably few strong reference points at the blue side of the spectrum (1335–1355 nm) at room temperature. To reduce errors from extrapolation of the calibration polynomial from points on the red side of the spectrum alone, the calibration was iterated by performing the same fitting process using a post-shock spectrum. After the initial calibration, the temperature of the measured spectrum was calculated as described below. Then new reference points were selected that covered almost the entire measured range (1335–1380 nm) from a high-temperature, post-shock measurement, and a new quadratic fit was performed. The new calibration was then used to determine a new temperature of the spectrum. This process was repeated until the temperatures before and after re-calibration were the same (usually one to two iterations). Calculated temperatures changed by 1–5% or 10–100 K between the first and second calibration.

Once a wavelength calibration was performed, determining temperature involved interpolating, smoothing, and differentiating both the measured and simulated spectra. A sample measured spectrum captured during the detonation of a 2.6 g PETN pellet is shown in figure 6 demonstrating these steps. Both the simulated and measured spectra were interpolated for comparison on a point-by-point basis and converted to the form of an absorption coefficient as indicated in figure 6(*a*). (Note that the measured spectrum is a not a true absorption coefficient due to the fact that it is based on I/I_{ref} rather than I/I_o.) The spectra were then smoothed using a Gaussian convolution of width 1.5 cm^{-1} (roughly 0.27 nm in the region studied) to eliminate high frequency noise and differentiated (figure 6(*b*)) to reduce lower frequency features and offsets due to differences in the structures of the baseline (I_{ref}) and transmission (I) signals. (These differences are currently attributed to polarization changes between the reference and transmitted signals and a polarization-dependent difference in system response after the reference and transmitted signals are recombined.) After processing, a measured spectrum was compared to each simulated spectrum across the range of temperatures in the

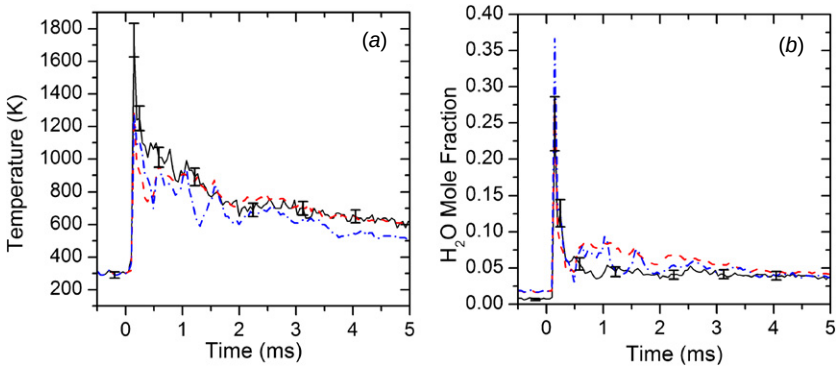

Figure 8. Water temperature (*a*) and mole fractions (*b*) calculated from transmission spectra after a 2.6 g charge of PETN was suspended at a setback distance of 23 cm. The shot-to-shot variation is indicated by these three replicate experiments.

database (250–3500 K) for the pressure that was measured at the time the transmission measurement was made. The mean-squared error (MSE) was calculated for each comparison, and the temperature that corresponded to the smallest MSE was taken as the measured temperature as shown in figure 7(*a*).

The simulated spectra used a reference mole fraction of 0.21 for the water vapor. When the shape of the simulated spectrum closely matched the shape of the measured spectrum near the best-fit temperature, the magnitude of each measurement or simulation point (α_{meas} or α_{sim}) still differed due to the ratio of the measured and simulated mole fractions (χ_{meas} and χ_{sim}, respectively). Following the form of equation (2), when pressure, temperature, lineshapes, linestrengths, and path length are known,

$$\frac{\alpha_{\text{meas}}}{\alpha_{\text{sim}}} = \frac{\chi_{\text{meas}}}{\chi_{\text{sim}}}. \tag{3}$$

A plot of the simulated versus the measured data points in the spectrum would thus reveal a linear trend, the best-fit slope of which represents the ratio of the measured mole fraction to the simulated mole fraction. Hence, the slope of the line of the simulated versus measured data was calculated for the temperatures nearest the best-fit temperature as shown in figure 7(*b*). Interpolation to the best-fit temperature (T_{bf}) as determined in figure 7(*a*) resulted in the multiplier that was used to calculate the mole fraction:

$$\chi_{\text{meas}} = 0.21 \times \text{slope}(T_{\text{bf}}). \tag{4}$$

This procedure was repeated for every measured spectrum. It is somewhat computationally cumbersome (and thus not suitable for real-time processing or high duty-cycle measurements), but it was adequate for determining temperatures and mole fractions in PETN detonation experiments described below.

3. Results

3.1. Temperature and mole fraction results

Results from three repeated experiments with a charge mass of 2.6 g, path length of 15 cm, and setback distance of 23 cm are displayed in figure 8. Temperature plots (figure 8(*a*)) displayed a general trend of a peak temperature of 1300–1700 K immediately after the shock, a quick decay to around 700–900 K within ∼1 ms, and finally a slow cooling to ambient conditions over tens of milliseconds (only data up to 5 ms shown). Mole fraction plots (figure 8(*b*)) displayed a similar trend of high initial mole fraction ∼0.25–0.4, a quick decay to around 0.05–0.1 within ∼0.25 ms, and finally a slower return toward ambient conditions over tens of milliseconds as surrounding air is entrained into the flow. (For comparison, a relative humidity of 45% equates to a water mole fraction of 0.01.) The data show 5–10% variation in temperature and 10–20% variation in mole fraction at any given time between the three tests.

Figure 9 shows temperature histories from PETN charges of 2.6 g at different setback distances and from a PETN charge of 21 g. Changing the setback distance from 15 to 23 cm is expected to cause a reduction in the measured temperature history due to weakening of the shock as it expands outward; however, the measured differences between the two experiments are of the same order as the variation in the repeatability data of figure 8. We thus cannot conclude a significant change in temperature with this change in measurement location. When the charge mass was increased by a factor of 8, the temperature profile was clearly elevated by a few hundred kelvin.

Finally, in figure 10, we present a comparison of the optical thermometer developed in this work with a type-R thermocouple of 50 μm diameter (Omega P13R-002) that has a time constant of 200 ms (in still air), according to the vendor. For this experiment, the thermocouple was placed directly next to the optically probed volume. The temporal advantage of the optical gauge is obvious in this comparison.

3.2. Uncertainty analysis

While the repeatability seems to be within 5–10% in temperature and 10–20% in mole fraction as indicated by figure 8, it is worth considering the experimental uncertainty of the technique and data reduction method in comparison to this shot-to-shot and charge-to-charge variability. To help quantify the uncertainty present in these measurements, several factors are considered: error propagated from smoothing the data, uncertainty in pressure, and wavelength calibration errors. We consider another potential source of error, inaccuracies in the

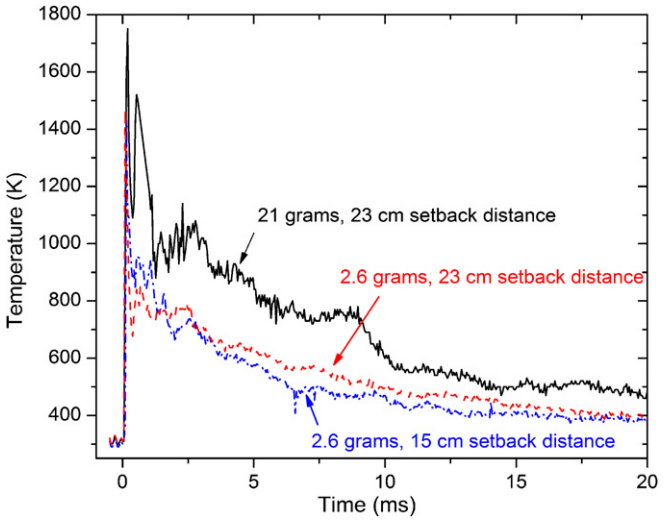

Figure 9. Comparison of measured water temperature with explosive charge mass and setback distance. While changing the setback distance had no significant effect on the small charges, the large charge clearly resulted in a higher temperature throughout the measurement time.

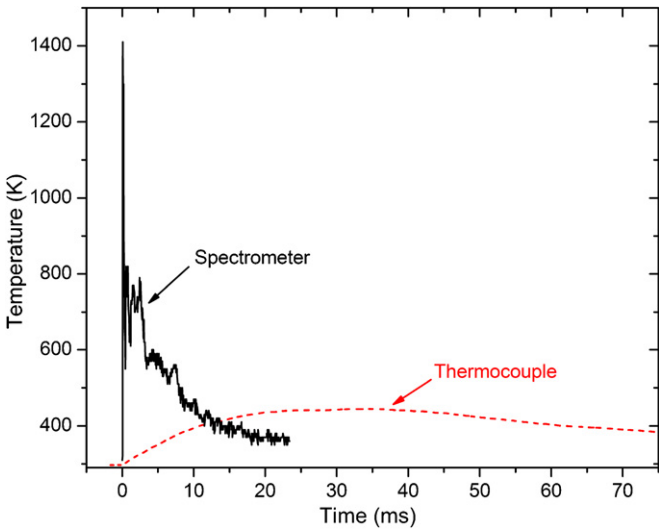

Figure 10. Comparison of the temporal response of the optically based water thermometer with a 50 μm type-R thermocouple. The charge mass was 2.6 g, and the setback distance was 15 cm.

spectral database, to be insignificant because of the large range of the spectrum investigated. That is to say, minor errors in single lines of the database should not drastically alter the final temperatures determined from the spectrum. We further believe that the BT2 database is the most complete of such lists available [19].

Smoothing of the measured data by convolving the data with a Gaussian profile of width 1.5 cm^{-1} ($\approx$0.27 nm) was performed to facilitate comparison between the measured and simulated spectra. To estimate the error associated with the selection of this width, temperatures and mole fractions were calculated using a range of widths from 0.5 to 2.5 cm^{-1}. These limits represent nominal bounds within which high frequency noise was eliminated and prominent absorption features remained. Errors associated with the smoothing of the spectra were determined to be $\pm$1–5% for temperature and $\pm$3–9% for mole fraction.

Error propagated by uncertainty in the measured pressure was also considered. Pressure traces showed an initial intense peak pressure that quickly decayed to nearly atmospheric pressure within roughly 100 μs after breakout. During this initial peak, average pressure measurements varied by up to 1 atm over the course of one measured spectrum (25 μs) (total peak pressures measured were, on average, 10 atm at the 15 cm setback). After pressures reached nearly atmospheric pressure, they changed by less than $\pm$0.1 atm over the course of a measured spectrum. To incorporate this uncertainty from pressure measurements, temperatures and mole fractions were recalculated by varying the pressure by 10% of the measured value. Temperatures determined in this manner were relatively unaffected by changes in pressure and generally displayed less than $\pm$1% variation. The mole fraction, being linearly dependent on pressure, carries a 10% uncertainty into the result.

The effect of uncertainty in the wavelength calibration was also considered. As mentioned above, the calibration was iteratively determined to minimize possible systematic errors; however the wavelength uncertainty due to the quadratic fit was $\pm$0.5 pixels ($\pm$0.025 nm) even after the iteration was performed. To estimate the uncertainty from the calibration, temperatures and mole fractions were recalculated after shifting the calibrated spectrum by $\pm$0.5 pixels. The resulting uncertainty is $\pm$1–3% in temperature and $\pm$1–4% of the measured mole fraction.

Using a root-mean-squared estimation, the overall amount of uncertainty from smoothing, pressure, and the calibration is estimated to be $\pm$2–6% for water temperatures and $\pm$10–15% for mole fractions. The temperature uncertainty is dominated by the Gaussian smoothing, while the mole fraction is an equally strong function of the assigned pressure and smoothing uncertainties. These uncertainties are only slightly smaller than the observed shot-to-shot variations in figure 8. Hence, the experiments seem to be repeatable to a degree that is close to the measurement uncertainty.

4. Discussion

The error analysis indicates that temperatures and concentrations can be measured with a good degree of confidence with uncertainty on the order of the shot-to-shot variation. The uncertainty estimated here is near the level of uncertainty of other techniques for fast temperature measurements in detonation environments such as pyrometry. However, pyrometry, in this case, suffers from low emission intensities following the detonation of the nearly oxygen balanced energetic PETN. Measurable pyrometry signals on this time scale require both higher temperatures and solid materials in the flow [18]. Furthermore, pyrometry measurements have known challenges associated with identifying the spatial location being measured due to changing optical thickness and the changing location of the emitting volume [3]. The chemical specificity of this

absorption technique promotes the measurement of the real-time internal energy conditions of a molecule in the flow as well as its concentration, which will be well suited to guide the development of chemically specific models in the future. While mole fraction measurements have uncertainties that are somewhat large (∼10%) in comparison to concentration measurements in more controlled environments, such as shock tubes and internal combustion engines [7, 21–23], the measurement error could be improved at the expense of time resolution.

Given the rather long path length (15 cm) used with this approach, noting that the results are path-averaged is important. Currently, the degree of uniformity across the path is unknown as the entrainment characteristics of the blast wave and detonation products are unknown. To obtain a more uniform probed volume, the path length can be reduced by incorporating wavelength modulation techniques, which would require a more sophisticated experimental setup than the current spectrometer, or by targeting molecules with stronger absorption coefficients, most likely with transitions in the visible and near UV. The spectrometer is convenient because of its ubiquity and its ease of adaptation to other wavelengths. Moving toward shorter wavelengths would also benefit from the use of streak camera detectors, which have excellent time resolution (∼1 ns). In order to accomplish this, other continuous-wave or high-repetition-rate light sources and components should be explored.

Since the shock travels an estimated 80 mm in 40 μs (the approximate period of one measurement cycle), the peak temperature at or near the shock front may slightly exceed the value measured with this technique. A visible streak camera, a shorter wavelength source, and a suitable tracer molecule might thus better resolve the peak temperature. This instrument would complement a streak-camera-based system with its ability to acquire much more data for a much longer period of time. Despite the acknowledged deficiencies in the time resolution of our approach, a continued investment of commercial technological advancement in this NIR wavelength region should help narrow the temporal gap between approaches (for example, a 100 kHz version of the array used in this study is already available for purchase).

The practicality of this measurement for detonation science and combustion science is shown to be reasonable in gram-scale explosive testing environments. Larger-scale, outdoor field testing of high explosives may be possible with further modifications to the gauge or the use of sacrificial gauges. The utility of this instrumentation with more applicable energetic materials that generate optically thick products is currently being investigated.

5. Conclusions

A fast, NIR absorption spectroscopy system, broadband light source, and rigid gauge have been constructed and combined to measure the temperature and concentration of water vapor as a detonation product within the expanding blast following the detonation of a solid, high explosive. To our knowledge, these are the first direct absorption measurements within the supersonic expansion regime following a detonation. This molecular thermometer exhibits a robust opto-mechanical design and a fast time response to measure the dynamic thermal fields of an explosive event. The data gathered from this instrument will further our understanding of detonation science by providing results that are directly comparable with species-specific models.

Acknowledgments

The authors would like to thank the Defense Threat Reduction Agency for funding this work. They would also like to thank Professor Scott Sanders for thoughtful discussions and insight shared during the experiment design stage. Robert Hay also has their gratitude for assisting with the explosive testing. Lastly, the authors would like to thank Dr Thomas P McGrath II for initial detonation science simulations which have aided in some of the design work and error analysis of this gauge. Future detonation science publications comparing these experimental results to simulations are in preparation.

References

[1] Taylor J 1952 *Detonation in Condensed Explosives* (Oxford: Clarendon)
[2] Lee J H S 2008 *The Detonation Phenomenon* (Cambridge: Cambridge University Press)
[3] Peuker J M, Lynch P, Krier H and Glumac N 2009 Optical depth measurements of fireballs from aluminized high explosives *Opt. Lasers Eng.* **47** 1009
[4] Carney J R, Lightstone J M, McGrath T P and Lee R J 2009 Fuel-rich explosive energy release: oxidizer concentration dependence *Propellants Explosives Pyrotechnics* **34** 331–9
[5] Carney J R, Miller J S, Gump J C and Pangilinan G I 2006 Time-resolved optical measurements of the post-detonation combustion of aluminized explosives *Rev. Sci. Instrum.* **77** 063103
[6] Musculus M P B, Singh S and Reitz R D 2008 Gradient effects on two-color soot optical pyrometry in a heavy-duty DI diesel engine *Combust. Flame* **153** 216
[7] Sanders S T, Baldwin J A, Jenkins T P, Baer D S and Hanson R K 2000 Diode-laser sensor for monitoring multiple combustion parameters in pulse detonation engines *Proc. Combust. Inst.* **28** 587–93
[8] Mattison D W, Brophy C M, Sanders S T, Ma L, Hinckley K M, Jeffries J B and Hanson R K 2003 Pulse detonation engine characterization and control using tunable diode-laser sensors *J. Propul. Power* **19** 568–72
[9] Lan C, Caswell A W, Kranendonk L A, Sanders S T, Urata Y and Okura Y 2007 19-color H_2O absorption spectrometer applied for real-time in-cylinder gas thermometry in an HCCI engine *SAE Paper* 2007-01-0188
[10] Kranendonk L A, Walewski J W, Kim T, Sanders S T, Burns I, Heatwole S and Alden M 2005 Wavelength-agile sensor applied for HCCI engine measurements *Proc. Combust. Inst.* **30** 1619–27
[11] Arroyo M P and Hanson R K 1993 Absorption measurements of water-vapor concentration, temperature, and line-shape parameters using a tunable InGaAsP diode laser *Appl. Opt.* **32** 6104–16
[12] Arroyo M P, Langlois S and Hanson R K 1994 Diode-laser absorption technique for simultaneous measurements of

multiple gasdynamic parameters in high-speed flows containing water vapor *Appl. Opt.* **33** 3296–307
[13] Glumac N, Krier H, Bazyn T and Ever R 2005 Temperature measurements of aluminum particles burning in carbon dioxide *Combust. Sci. Technol.* **177** 485–511
[14] Carney J R, Wilkinson J and Lightstone J M 2007 Time-resolved optical measurements of detonation and combustion products *Shock Compression of Condensed Matter—2007, AIP. Conf. Proc.* **955** 1225–8
[15] Glumac N 2009 Absorption spectroscopy measurements in optically dense explosive fireballs using a modeless broadband dye laser *Appl. Spectrosc.* **63** 1075
[16] Kranendonk L A, Caswell A W and Sanders S T 2007 Robust method for calculating temperature, pressure, and absorber mole fraction from broadband spectra *Appl. Opt.* **46** 4117–24
[17] Conrad B and Sanders S 2009 Delayed pulse referencing for cancellation of polychromatic beating noise in grating spectrometry *Appl. Phys.* B **96** 715
[18] Koch J D, Piecuch S, Lightstone J M, Carney J R and Hooper J 2010 Time-resolved measurements of near infrared emission spectra from explosions: pure pentaerythritol tetranitrate and its mixtures containing silver and aluminum particles *J. Appl. Phys.* **108** 036101
[19] Barber R J, Tennyson J, Harris G J and Tolchenov R N 2006 A high-accuracy computed water line list *Mon. Not. R. Astron. Soc.* **368** 1087–94
[20] Wells R 1999 Rapid approximation to the Voigt/Faddeeva function and its derivatives *J. Quant. Spectrosc. Radiat. Transfer* **62** 29–48
[21] Cai T, Jia H, Wang G, Chen W and Gao X 2009 A sensor for measurements of temperature and water concentration using a single tunable diode laser near 1.4 μm *Sensors Actuators* A **152** 5
[22] Rieker G B *et al* 2007 Rapid measurements of temperature and H_2O concentration in IC engines with a spark plug-mounted diode laser sensor *Proc. Combust. Inst.* **31** 3041
[23] Mattison D W, Jeffries J B, Hanson R K, Steeper R R, De Zilwa S, Dec J E, Sjoberg M and Hwang W 2007 In-cylinder gas temperature and water concentration measurements in HCCI engines using a multiplexed-wavelength diode-laser system: sensor development and initial demonstration *Proc. Combust. Inst.* **31** 791–8